New observational constraints on warm rain processes and their climate implications

Xiquan Dong[1], Peng Wu[1], Yuan Wang[2,3], Baike Xi[1], and Yiyi Huang[1]

1. Department of Hydrology and Atmospheric Sciences, University of Arizona, Tucson, AZ, 85710, USA
2. Division of Geological and Planetary Sciences, California Institute of Technology, Pasadena, CA, USA
3. Jet Propulsion Laboratory, California Institute of Technology, Pasadena, CA, USA

Revision to *Geophysical Research Letters*

Fenruary 11, 2021

Main points:

1. Constrain a microphysics scheme using new cloud and drizzle retrievals
2. Implemented the updated scheme in NCAR CESM to simulate the warm rain globally
3. The updated scheme alleviates a long-lasting problem in most climate models

Corresponding author address: Dr. Xiquan Dong, The Department of Hydrology and Atmospheric Sciences, University of Arizona, 1133 E. James Rogers Way, PO Box 210011, Tucson, AZ 85721-0011, USA. Email: xdong@arizona.edu; Phone: 520-621-4652.

Abstract:

Low stratiform clouds have profound impacts on the hydrological cycle and the Earth's radiation budget. However, realistic simulation of low clouds in climate models presents a major challenge. Here we employ the newly retrieved cloud and drizzle microphysical properties to improve the autoconversion and accretion parameterizations in a microphysical scheme. We find that the new autoconversion (accretion) rate contributes 14% lower (greater) to total drizzle water content than the original scheme near the cloud top. Compared to satellite results, the simulated cloud liquid water path (LWP) and shortwave cloud radiative effect using the original scheme in a climate model agree well on global average but with large regional differences. Simulations using the updated scheme show a 7.3% decrease in the light rain frequency, and a 10% increase in LWP. The updated microphysics scheme alleviates the long-lasting problem in most climate models, i.e. 'too frequent and too light precipitation'.

Plain-language summaries

There has been a growing concern that most climate models predict too frequent and too light precipitation, which is primarily due to lack of reliable sub-grid variability and vertical variations of microphysical processes in low clouds. With the newly retrieved cloud and drizzle microphysical properties from a recent field campaign, we updated the classic warm rain microphysical scheme which was developed by Khairoutdinov & Kogan (2000) and widely used in weather and climate models. We examined relative contributions of different microphysical processes to the rain drop formation and growth processes. The altered scheme reflects the advance in process-level understanding of warm rain processes and reveals their relative contributions to the rain drop formation and growth processes at different cloud heights. The altered scheme has the potential of mitigating the long-lasting problem in most climate models and achieving more accurate climate assessments. Our findings unambiguously attest the paramount importance of cloud microphysical parameterizations in climate simulation.

1. Introduction

Low-level stratiform clouds (hereafter called low clouds) have been a topic of considerable interest because they strongly reflect incoming shortwave radiation (Stephens et al., 2015) and exert complex feedbacks on the climate system (Stephens, 2005; Wood, 2012; IPCC, 2013; L'Ecuyer et al., 2019; Hang et al. 2019). The radiative effect of low clouds contributes to one of the largest uncertainties in climate modeling (Stephens et al., 2015; IPCC, 2013) and has been well known to be influenced by aerosols (Penner et al., 2004; Ghan et al., 2016; Seinfeld et al., 2016; Fan et al., 2016; Li et al., 2020). Drizzle is common in maritime low clouds (Dong et al., 2014 a&b; Wu et al., 2015 & 2017). The formation of drizzle significantly modulates stratocumulus-to-cumulus transition (Yamaguch et al., 2017) and plays an important role in determining cloud lifetime (Albrecht, 1989). Furthermore, they have profound impacts on the hydrological cycle and the Earth's radiation budget (Stephens et al., 2015; Wood et al., 2009; Stephens et al., 2010; Suzuki et al., 2010; Kay et al., 2018), and consequently on the Earth's climate (Bony et al., 2005; Schmidt et al. 2006). Despite their importance, it is challenging to simulate low clouds realistically in climate models where they disagree substantially in the magnitude of cloud feedback for the regimes of low clouds. As a result, most general circulation models (GCMs) predict too frequent and too light precipitation (Stephens et al., 2010; Donner et al. 2011; Soden et al., 2011; Lebsock et al., 2013; Jing et al., 2017 & 2018; Wu et al., 2018; Zhang et al., 2019).

Another great challenge in GCMs is how to evaluate the cloud microphysical processes, such as autoconversion (R_{auto}) and accretion (R_{accr}) rates in low clouds (Wu et al., 2018; Zhang et al., 2019) since these processes cannot be directly measured. In fact, these processes are often parameterized as power law relationships with cloud and drizzle properties in model simulations. Satellite results have been widely used to evaluate these processes and concluded that GCM simulations are very sensitive to the choices of threshold cloud droplet radius in simulating the cloud-to-rain particle conversion and growth processes (Suzuki et al., 2010, 2013 & 2015; Nakajima et al., 2010). However, satellite retrievals suffer relatively large uncertainties, originating from their measurement and retrieval errors, as well as their limitations in observing clouds, especially for drizzling clouds (Suzuki et al., 2010; Ma et al., 2018). Most GCMs predict too frequent and too light precipitation due to lack of reliable sub-grid variability and vertical variations of R_{auto} and R_{accr} (Jing et al., 2017; Wu et al., 2018; Zhang et al., 2019; Suzuki et al., 2010; Golaz et al., 2002; Liu et al., 2007; Cheng and Xu, 2009; Wood and Hartmann, 2006).

The retrieved cloud and drizzle microphysical properties during the Aerosol and Cloud Experiments in the Eastern North Atlantic (ACE-ENA) field campaign (Wu et al., 2020) have 1-min temporal and 30-m vertical resolution, which are important for studying warm rain processes. In this study, we used the retrievals to recalibrate the R_{auto} and R_{accr} parameterizations in Khairoutdinov & Kogan (2000) scheme (hereafter called KK) into the new KK scheme (hereafter called NKK). The profiles of R_{auto} and R_{accr} ($R_{auto}(Z)$ and $R_{accr}(Z)$, where Z is the in-cloud height) can be used to advance the process-level understanding of warm rain process. To further test the NKK scheme, we implemented the $R_{auto}(Z)$ and $R_{accr}(Z)$ into the National Center for Atmospheric Research (NCAR) Community Earth System Model (CESM, Morrison and Gettelman, 2008; Hurrell et al., 2013) to simulate the warm rain frequency and intensity globally.

2. Methods

2.1 Recalibrate the KK warm rain scheme

A brief summary about the ground-based retrieval (Wu et al., 2020) is presented in the supplementary. The retrieved microphysics include cloud-droplet (drizzle) number concentration N_c ($N_d(Z)$) liquid water content LWC_c(Z) (LWC_d(Z)) and mass weighted mean radius r_c(Z) (= $\left(\frac{3LWC_c}{4N_c\pi\rho_w}\right)^{1/3}$) and r_d(Z). The units of LWC, r, and N in this study are gm^{-3}, μm, and cm^{-3}, respectively. Figures S1a-S1d show the retrieved cloud and drizzle microphysical properties. The retrieved LWC_c(Z) and r_c(Z) increased from the cloud base, peaked just below the cloud top, and then decreased toward the cloud top. The retrieved r_d(Z) and LWC_d(Z) (Figs. S1c & S1d), opposite to their cloud counterparts, increased from the cloud top downward, peaked in the middle or bottom of the cloud, and decreased further down.

The R_{auto} and R_{accr} are usually parameterized as power law relationships with cloud and rain water mixing ratios (q_c and q_r) and N_c (KK; Kessler, 1969; Tripoli et al., 1980; Beheng, 1994; Liu and Daum, 2004), and in the forms of

$$R_{auto}(Z) = \left(\frac{\partial q_r}{\partial t}\right)_{auto} = \mathrm{A}\, q_c^{a1}(Z) N_c^{a2}, \qquad (1)$$

$$R_{accr}(Z) = \left(\frac{\partial q_r}{\partial t}\right)_{accr} = B\, (q_c(Z) q_r(Z))^b, \qquad (2)$$

where A, $a1$, $a2$, B, and b are coefficients in different schemes and are usually constants. In this study, q_c(Z) and q_r(Z) can be calculated from retrieved LWC_c(Z) and LWC_d(Z) and dry air density (ρ_{air}), therefore, $R_{auto}(Z)$ and R_{accr}(Z) are a function of height Z in Eqs. (1) and (2). In addition to

LWC_c(Z) and LWC_d(Z), the retrieved layer-mean N_c is also used in Eq. (1). As a proof of concept, the KK scheme is used as an example in this study, in which $A = 1350$, $a1 = 2.47$, $a2 = -1.79$, $B = 67$, and $b = 1.15$.

The summation of R_{auto}(Z) and R_{accr}(Z) is the total drizzle water production rate (P_r(Z)), which can be converted to LWC_d(KK) ($= \int \rho_{air} P_r(Z) * dt$, dt is 1 min here) to directly compare with retrieved LWC_d(Z) with 1-min temporal resolution.The retrieved LWC_d(Z) is then used to scale the time interval of $LWCd$(KK) within 1 minute as

$$R'_{auto}(Z) = \frac{LWC_d(Z)}{\int \rho_{air} P_r\,(Z)dt} R_{auto}(\mathrm{Z}) = \mathrm{A}'(\mathrm{Z}) q_c^{2.47}(Z) N_c^{-1.79}, \quad (3)$$

$$R'_{accr}(Z) = \frac{LWC_d(Z)}{\int \rho_{air} P_r\,(Z)dt} R_{accr}(Z) = B'(Z)(q_c(Z) q_r(Z))^{1.15}. \quad (4)$$

A'(Z) and $B'(Z)$, which are functions of height Z with unitless, can be calculated from Eq. (3) and Eq. (4). To clarify the terms used in this study, $R_{auto}(Z)$ and $R_{accr}(Z)$, and constants A and B are used in KK scheme, while $R'_{auto}(Z)$ and $R'_{accr}(Z)$, and $A'(Z)$ and $B'(Z)$ are used in NKK scheme.

A sensitivity study has shown that the coefficients A and B in Eqs. (1) and (2) are more or less dependent on the retrieved r_c and r_d than other coefficients $a1$, $a2$, and b. Also, because of the linear constraining in Eq. (3) and Eq. (4), the linear coefficients A and B are modified in this study and the exponential terms are retained. The relationship between q_c and N_c in KK does constrain r_c, but this constraint seems too weak in the lower part of cloud and too strong in the upper (Fig. S1f).

The $LWC_d(KK)$ profiles peaked in the center and upper part of the cloud (Fig. S1e), which are different from the retrieved LWC_d(ret). The ratios of LWC_d (KK) to LWC_d (ret) (Fig. S1f) show that LWC_d (KK) were overestimated in the upper part and underestimated in the lower part of the cloud. The higher LWC_d ratios in the upper part and reduced ratios in the lower part of the cloud suggest that it is imperative to recalibrate and constrain the KK scheme using observations. The profiles of the LWC_d ratios in Fig. S1f motivate us to modify the coefficients A and B as a function of height Z, such as $A'(Z)$ and $B'(Z)$, not constants with height. Physcially, $A'(Z)$ and $B'(Z)$ should strongly correlate with the profiles of cloud and drizzle microphysical properties, more precisely, to $r_c(Z)$ and $r_d(Z)$.

Note that KK scheme is used as an example in this study in which we first calculate P_r(Z) by summing R_{auto}(Z) and R_{accr}(Z), and then constrain the original R_{auto}(Z) and R_{accr}(Z) with retrieved LWC_d(Z) in Eq. (3) and Eq. (4). The approaches can only be applied to schemes having both R_{auto}

and R_{accr} parameterizations, while those having one of them, such as having A_{auto} in Liu and Daum (2004), cannot be modified in this study.

2.2 CESM Simulations

The NSF/DOE Community Earth System Model (CESM) version 1.2.2 (Hurrell et al., 2013) is used in this study to access the impacts of altered warm rain microphysics on cloud and precipitation on the regional and global scale. The atmospheric component, Community Atmosphere Model version 5.3 (CAM5), possesses notable improvements in simulating cloud and precipitation. In particular, a prognostic two-moment stratiform cloud microphysics scheme (Morrison and Gettelman, 2008) was implemented in the CAM5 for the first time. The KK scheme is used for the warm rain process.

Six-year equilibrium present-day forcing simulations (2000-2005) are performed for each microphysical configuration. The first year (2000) is considered as spin-up, and the last five-year results (2001-2005) are analyzed. To assess the Probability Density Function (PDF) of precipitation rates, typically high frequency (e.g., hourly) precipitation output is required. However, it is computationally expensive to store such high-frequency output in a global climate model. In this study, we adopted an in-situ diagnostic method (Wang et al., 2016) to generate precipitation probability density functions (PDFs) based on rain rates at each model time step (the hourly time scale) because this method can also facilitate the comparison between GCM simulated and satellite retrieved transient precipitation rates (Aumann et al., 2018).

3. Constrain cloud microphysics scheme using ground-based retrievals

The R_{auto}(Z)and R_{accr}(Z) profiles, calculated from ground-based retrievals using Eqs. (1) and (2), for the case of July 18, 2017 are presented in Fig. S2. As expected, R_{auto}(Z) increases with height, basically follows the LWC_c(Z) profiles. During drizzle drops falling process, $R_{accr}(Z)$ becomes increasingly important as demonstrated in Fig. S2b where R_{accr}(Z) is the largest in the cloud center. To recalibrate R_{auto}(Z) and R_{accr}(Z) in the KK scheme, we used the retrievals to derive $A'(Z)$ and $B'(Z)$ profiles as demonstrated in Figs. S2c & S2d. Figures 1a and 1b show the probability density functions (PDFs) and cumulative density functions (CDFs) of $A'(Z)$ and $B'(Z)$. The prescribed A and B values (constants) in the KK scheme fall in the same bins as their mode values, suggesting that the prescribed values are representative for the most scenarios.

To be applicable of $A'(Z)$ and $B'(Z)$ in model simulations, we parameterized $A'(Z)$ and $B'(Z)$ as exponential functions of $r_c(Z)$ and $r_c(Z)/r_d(Z)$ in Figs. 1c and 1d as:

$$A'(Z) = 121683\exp(-0.528\, r_c(Z)) + 364, \tag{5}$$

$$B'(Z) = 632\exp\left(-24.5\frac{r_c(Z)}{r_d(Z)}\right) + 51. \tag{6}$$

The profiles of $A'(Z)$ and $B'(Z)$ in Fig. S2 are smaller than their prescribed values in the upper part and greater in the lower part of the cloud. The joint PDFs of $A'(Z)$ and $r_c(Z)$ with an exponential relationship between them (Eq. 5) are illustrated in Fig. 1c. We find that $A'(Z)$ decreases with increasing $r_c(Z)$ and becomes smaller than the prescribed A when $r_c(Z)$ is greater than ~9 μm. Physically, R_{auto} should increase with increasing $r_c(Z)$, the result here suggests that the power law functions for $q_c(Z)$ and N_c in Eq. (1) are too strong and the fitted exponential formula $A'(Z)$ acts to reduce the power law relationship and bring $R'_{auto}(Z)$ to more reasonable values to correct the overestimated $LWC_d(KK)$ in the upper part and underestimated $LWC_d(KK)$ in the lower part of the cloud as shown in Fig. S1f. Introducing $r_c(Z)$ in Eq. (3) adds a more direct constraint on the autoconversion process than the relationship originally used in KK because the autoconversion process is primarily a conversion process from cloud droplets to drizzle drops near the cloud top.

Similarly, we fitted an exponential function between $B'(Z)$ and $r_c(Z)/r_d(Z)$ (Eq. 6) in Fig. 1d. $B'(Z)$ decreases with increasing $r_c(Z)/r_d(Z)$ until the ratios reach ~0.2. The fitted formula and the pattern of the joint PDF, as well as Fig. S1f, reveal that $B'(Z)$ values should change with height. Near the cloud top, $r_c(Z)$ is the largest while $r_d(Z)$ is the smallest, resulting in the greatest $r_c(Z)/r_d(Z)$, where $B'(Z)$ from the NKK scheme are the smallest and remain nearly constant (~50) for $r_c(Z)/r_d(Z) > 0.2$, even smaller than the prescribed B (B=67). From the cloud top to the cloud base, $r_c(Z)$ decreases but $r_d(Z)$ increases, resulting in the smallest $r_c(Z)/r_d(Z)$ at the bottom of the cloud. $B'(Z)$ increases with decreasing $r_c(Z)/r_d(Z)$ from the top to the base and reaches the largest value at the bottom of the cloud. This change in $B'(Z)$ will counterbalance the overestimated $LWC_d(KK)$ in the upper part and underestimated $LWC_d(KK)$ in the lower part of the cloud as demonstrated in Fig. S1f.

Theoretically, the collision efficiency is the highest and reaches nearly unity for $r_c(Z)/r_d(Z) > 0.2$, while the collision efficiency decreases significantly with decreasing $r_c(Z)/r_d(Z)$ (Rogers and Yau, 1989). With fixed drizzle drop size, larger cloud droplets have higher collision efficiency and correspondingly larger R_{auto} values, which typically happens near the cloud top. For smaller cloud droplets, their collision efficiencies are much lower because they tend to follow the streamlines around a falling drizzle drop. However, the coalescence efficiency is opposite to the collision efficiency, that is, smaller cloud droplets more easily stay with drizzle drops and remain joined. This argument is further proved from the retrieved r_c(Z), $r_d(Z)$, $LWC_c(Z)$ *and* LWC_d(Z) in Fig. S1 and R_{auto} and R_{accr} in Figs. 1e and 1f. R_{auto} contribution to drizzle water content increases with height, peaking near the cloud top which basically follows the r_c(Z) and LWC_c(Z) variations, while R_{accr} contributes most near the cloud base which is attributed by r_d(Z) and LWC_d(Z).

The fitted exponential formula between $B'(Z)$ and $r_c(Z)/r_d(Z)$ in Fig. 1d is opposite to the theoretical collision efficiency. This is because the KK scheme tends to overestimate LWC_d(KK)near the cloud top and $B'(Z)$ should be decreased in order to lessen R_{accr}. Near the cloud base, $B'(Z)$ is usually the largest from the NKK scheme, which acts to enhance R_{accr} to compensate the underestimation of LWC_d (KK).

For warm rain processes, cloud droplets normally form at the cloud base, grow with height through condensation in updrafts into the largest cloud droplets (r_c~20 µm, Rogers and Yau, 1996; Wood, 2005a&b; Wallace and Hobbs, 2006; Takahashi et al., 2017), and become drizzle-sized drops through the collision-coalescence near the cloud top in which R_{auto} becomes important (Wu et al., 2015; Cheng and Xu, 2009; Liu and Daum, 2004, Wu et al., 2015). These drizzle drops fall from near the cloud top grow by collecting cloud droplets and small drizzle drops. As drizzle drops fall, R_{accr} becomes increasingly important.

To quantify the cloud-to-rain particle conversion and growth processes, we normalized the individual profiles in cloud height coordinate. R_{auto}(Z) and A_{accr}(Z) are calculated from prescribed A and B (constants, white dashed lines in Figs. 1c and 1d) in the KK scheme, while the NKK scheme $A'(Z)$ and $B'(Z)$ are function of r_c(Z) and $r_c(Z)/r_d(Z)$ as shown in Figs. 1c and 1d (solid while lines). Figure 1e shows the composite profiles of R_{auto} and R_{accr} for all the drizzle cases during ACE-ENA. The normalized R_{auto} increased significantly with height, with a peak at $z_i \sim$ 0.75, and then decreased toward the cloud top. The smaller R_{auto} values at the cloud top are mainly caused by cloud droplet evaporation associated with cloud-top entrainment as observed by aircraft in situ measurements (Wu et al., 2020). The normalized R_{accr} values are, in general, one order of magnitude greater than the R_{auto} except at the cloud top where they are closer. The $R'_{auto}(Z)$ values are slightly less than the R_{auto}(Z) values in the upper part of the cloud and greater in the lower part. The $R'_{accr}(Z)$ values, on the other hand, are greater than the R_{auto}(Z) values at all levels.

The relative contributions of R_{auto} and R_{accr} to total drizzle water production rate ($P_r = A_{auto} + A_{accr}$) are presented in Fig. 1f. R_{auto}(Z) and R_{accr}(Z) contribute ~45% and 55% of $P_r(Z)$ near the cloud top, respectively. As drizzle drops fall, R_{accr} becomes increasingly important. For the NKK scheme, the $R'_{auto}(Z)$ and $R'_{accr}(Z)$ contribute ~31% and ~69% of P_r(Z) near the cloud top, which are 14% less and more, respectively, than the contributions from the KK scheme. The relative contributions of autoconversion (accretion) gradually decrease (increase) toward the cloud base and have nearly the same in both schemes below $z_i = 0.3$. Near the cloud top, the 14% lower contribution from $R'_{auto}(Z)$ corroborates that the NKK scheme has lower precipitation frequency than the KK scheme. On the other hand, the 14% greater contribution from $R'_{accr}(Z)$ confirms that the NKK scheme has higher precipitation intensity than the KK scheme. At the upper part of the clouds, the less (more) autoconversion (accretion) contributions from the NKK scheme corroborate the notion that the KK scheme overestimated autoconversion rates and underestimated accretion rates, which could be a reason that most GCMs predict 'too frequent and too light precipitation'. Meanwhile, the NKK scheme has the potential to mitigate the outstanding problem in GCM precipitation simulations and shed light on future model development.

Notice that the focus of this study is on the vertical distributions of R_{auto} and R_{accr}, and their impacts on precipitation simulation. The spatial variations of R_{auto} and R_{accr}, especially their subgrid variabilities, should share the equal importance in precipitation simulation. For example, Wu et al. (2018) calculated the so-called enhancement factors, E_{auto} and E_{accr}, using ARM ENA ground-based observations and retrievals. They found both enhancement factors increase with the increase of model grid size. These results are similar to those from Xie & Zhang (2015) and results from satellite observations in Lebsock et al. (2013) and Zhang et al. (2019). Comparing the prescribed enhancement factors in Morriosn and Gettelman (2008) to the observed ones, a higher E_{auto}(3.2) and a lower E_{accr}(1.07) at small grids were used in Morriosn and Gettelman (2008). In this study, however, we only investigate the vertical distribution of A_{auto} and A_{accr} and their impact on precipitation with prescribed enhancement factors in CESM simulations.

4. Impacts of the updated microphysics scheme in climate simulations

The KK scheme has been widely used in cloud-resolving (Seinfeld et al., 2016) and global climate models, including the NCAR/DOE CESM (Morriosn and Gettleman, 2008; Hurrell et al., 2013; Gettleman et al., 2019). In this study, we implemented the updated schemes $R'_{auto}(Z)$ and $R'_{accr}(Z)$ in CESM version 1.2 (CESM1) to assess the climatic influence of recalibrated cloud microphysical processes. We first compare the standard CESM1 simulations with the satellite products to justify the rationale of updating microphysics scheme. The CERES Edition 4 cloud liquid water path (LWP) retrievals from the Moderate Resolution Imaging Spectroradiometer (MODIS) and shortwave cloud radiative forcing (SWCF) from the Clouds and the Earth's Radiant Energy System (CERES) on board of the Terra and Aqua satellites (Minnis et al., 2020) will serve as the benchmark. Figure 2 shows the CESM1 simulated spatial distributions of maritime LWPs between 60º S and 60º N with a mean of 43.0 g/m^2, which is close to the satellite retrieval (44.1 g/m^2). However, large differences exist over some regions. For example, there are positive biases of LWP in CESM1 over the Inter Tropical Convergence Zone (ITCZ), whereas over the stratocumulus-prevailing regions like the Southeast Pacific and Southeast Atlantic, the negative biases can be up to -20 g/m^2 as shown in Fig. 2e., which is consistent with the common problem of GCM, i.e., too frequent drizzle precipitation for stratus and stratocumulus clouds.

The spatial distributions of observed and modeled SWCF values have strong negative correlations with their corresponding LWPs, that is, larger LWP corresponds to stronger negative SWCF as illustrated in Figs. 2b and 2d. The spatial distribution of the biases in SWCF (Fig. 2f) mirrors those in LWP (Fig. 2e), indicating that the SWCF biases are largely contributed by those in LWP. Over 60º S to 60º N, the oceanic SWCF bias is -2.3 W/m^2. In addition to CESM1 simulations, we also simulate cloud LWP using CESM2 (version 2.1.1) whose microphysical scheme includes an enhancement factor in the KK scheme. However, the LWP in CESM2 is found to be overestimated by 66% in comparison with satellite observations (Fig. S3). Therefore, we choose not to test our observational constraints in CESM2.

To reveal the relative importance of the changes in R_{auto} and R_{accr} parameterizations, we conducted two model sensitivity studies by using $R'_{auto}(Z)$ first, and then using both $R'_{auto}(Z)$ and $R'_{accr}(Z)$ in CESM1. Figure 3a shows the differences in maritime stratiform cloud LWP between the simulations using $R'_{auto}(Z)$ and R_{auto}(Z) in which $R'_{auto}(Z)$ significantly increased cloud LWP. Such an increase is more evident in the mid-latitude regions than the tropics, which can be attributed to the fact that the stratiform clouds are more prevalent in the mid-latitudes. The increased *LWPs* in the mid-latitudes using NKK greatly counterbalance the negative biases in LWP using KK scheme (Fig. 3e), bring the modeled LWPs closer to satellite retrievals. In particular, the simulated LWPs using $R'_{auto}(Z)$ increased 11.8 g m^{-2} over 60º S-60º N oceanic regions (Fig. 3a) which is more than 20% fractional changes, and 9.8 g m^{-2} globally (Fig. S4b). The increases in mean stratiform cloud fractions (CFs) were only 0.5% and 0.8% for the mid-latitudes and globally (Fig. S5), but much more for fractional changes, up to 10% over the regions like subtropics and the Arctic as seen in Fig. S5d.

The reduced $R'_{auto}(Z)$ near the cloud top shown in Fig. 1f corroborates the notion that the overestimation of R_{auto} is more important in determining the overall R_{auto} effect than the underestimation of R_{auto} in the bottom of the cloud. Hence, $R'_{auto}(Z)$ exerts a larger influence on the height dependency of precipitation processes in the cloud. In contrast, R_{accr} is generally underestimated throughout the whole cloud profile (Figs. 1e and 1f). Therefore, a stronger $R'_{accr}(Z)$ can be expected when implementing it in the model simulations, which can result in more cloud LWP as evident in Fig. 3a. Taking changes by both $R'_{auto}(Z)$ and $R'_{accr}(Z)$ into account together, the net cloud LWP changes (Fig. 3b) are much less than those simulated with $R'_{auto}(Z)$ only in Fig. 3a, but are still dominated by the impact of the autoconversion change, with a mean increase of 4.5 g m^{-2} over 60º S-60º N oceanic regions, corresponding to a 10% increase. No significant changes in stratiform CFs using $R'_{auto}(Z)$ only or both $R'_{auto}(Z)$ and $R'_{accr}(Z)$ are found in this study (Fig. S5).

Cloud-to-rain particle conversion is also crucial for drizzle formation process in clouds. With suppressed autoconversion rates near the cloud top, the $R'_{auto}(Z)$ results in significant reductions in precipitation frequency, particularly in the subtropical regions (Figs. S4c and S4d). Figure S4d illustrates the decreased precipitation frequency corresponded with increased cloud LWP (Fig. S4b) and stratiform CF (Fig. S5), although they were imperfectly matched in their spatial distributions. Similar to the cloud responses, the rain formation process is dominated by the autoconversion change. This conclusion is further confirmed in Figs. S4c and S4d where the mean absolute changes in global precipitation frequency are -3.1% with $R'_{auto}(Z)$ only and -2.6% with both $R'_{auto}(Z)$ and $R'_{accr}(Z)$, with a significant decrease over the tropical regions.

To further probe the surface precipitation changes as a function of rain intensity, we employed an in situ diagnostic method (Wang et al., 2016) to generate precipitation PDFs based on rain rates on the hourly time scale. During the model integration, at each model time step, the new diagnostic accumulates instantaneous precipitation rates into 30 predefined bins. At the end of each month, the corresponding percentage for each bin can be calculated to obtain a PDF and output it in the monthly data. The model sensitivity run shows that for the stratiform clouds, the mean frequency of drizzle or light precipitation (intensities less than 5 mm/day) was reduced from 25.2% to 22.7% when $R'_{accr}(Z)$ was applied (Fig. 3e), corresponding to a 10% fractional decrease. With an elevated accretion rate in the NKK scheme updating both processes, a 7.3% (fractional) drizzle reduction still exists. The reduced precipitation frequency with the NKK scheme alleviates a long-lasting problem related with the precipitation in GCMs (Stephens et al., 2010). It is difficult to obtain stratiform precipitation from observations, so we do not compare the stratiform precipitation PDF with observations in this study. Wang et al. (2016) examined the total precipitation PDF in the CESM1 simulations using the KK scheme, and found that the simulated precipitation frequency for light precipitation frequency is 5% higher than the Tropical Rainfall Measuring Mission (TRMM, Lau and Wu, 2011) observations (54%) over the tropical region of 25° S-25° N. Although it is not the same region as this study (60° S-60° N), this result corroborates that the simulated precipitation frequency using the NKK scheme is changing towards to observed one.

5. Conclusions

It is a great challenge to realistically simulate low clouds and associated warm rain in climate models without reliable vertical variations of microphysical processes. In this work, we use the newly retrieved cloud and drizzle microphysical properties to constrain the autoconversion and accretion parameterizations in a widely used microphysical scheme, and then implement the updated scheme into the NCAR CESM to examine the responses of warm rain frequency and cloud properties. Climate simulations with the updated cloud microphysical scheme exhibit the reduced precipitation frequency and increased precipitation intensity, indicating that the new scheme has the potential of mitigating the outstanding problem in GCM precipitation simulations and achieving more accurate climate assessments.

The findings from this study attest the paramount importance of cloud microphysics parameterizations in GCM simulations. In particular, we show that it is critical to take the in-cloud vertical variations of warm rain processes into account when developing cloud microphysical schemes. We note that the robustness of our findings is subject to the representative of new parameterizations derived from a field campaign. Therefore, it is imperative to use more ground-based observations from different field campaigns and ARM permanent sites as well as a single column modeling framework to test if these new parameterizations are valid over other oceans and land surfaces. Future study will also focus on how altered warm rain processes can influence the aerosol indirect effect, cloud feedback, and climate sensitivity.

Acknowledgements

This research was supported by the NSF project under grant AGS-1700728/AGS-2031750 at the University of Arizona and AGS-1700727/AGS-2031751 at California Institute of Technology. The researchers at the University of Arizona were also supported as part of the "Enabling Aerosol-cloud interactions at GLobal convection-permitting scalES (EAGLES)" project (74358), funded by the U.S. Department of Energy, Office of Science, Office of Biological and Environmental Research (BER), Earth System Modeling program with the subcontract to the University of Arizona. Y.W. acknowledges the support of the Jet Propulsion Laboratory, California Institute of Technology, under contract with NASA. Measurements during ACE-ENA IOP were obtained from the Atmospheric Radiation Measurement (ARM) Program sponsored by the U.S. Department of Energy (DOE) Office of Energy Research, Office of Health and Environmental Research, and Environmental Sciences Division. The data can be downloaded from http://www.archive.arm.gov/.

References

Albrecht, B. A. Aerosols, Cloud Microphysics, and Fractional Cloudiness. *Science.* **245** (4923), 1227–1230 (1989).

Aumann, H. H., Behrangi, A. & Wang, Y. Increased Frequency of Extreme Tropical Deep Convection: AIRS Observations and Climate Model Predictions. *Geophys. Res. Lett.* **45**, 13,530-13,537 (2018).

Beheng, K. D. A parameterization of warm cloud microphysical conversion processes. *Atmos. Res.* **33**, 193–206 (1994).

Bony, S. & Dufresne, J. L. Marine boundary layer clouds at the heart of tropical cloud feedback uncertainties in climate models. *Geophys. Res. Lett.* **32**, 1–4 (2005).

Cheng, A. & Xu, K.-M. A PDF-Based Microphysics Parameterization for Simulation of Drizzling Boundary Layer Clouds. *J. Atmos. Sci.* **66**, 2317–2334 (2009).

Dong, X., Xi, B., Kennedy, A., Minnis, P. & Wood, R. A 19-Month Record of Marine Aerosol–Cloud–Radiation Properties Derived from DOE ARM Mobile Facility Deployment at the Azores. Part I: Cloud Fraction and Single-Layered MBL Cloud Properties. *J. Clim.* **27**, 3665–3682 (2014a).

Dong, X. *et al.* Investigation of the Diurnal Variation of Marine Boundary Layer Cloud Microphysical Properties at the Azores. *J. Clim.* **27**, 8827–8835 (2014b).

Donner, L. J. *et al.* The dynamical core, physical parameterizations, and basic simulation characteristics of the atmospheric component AM3 of the GFDL global coupled model CM3. *J. Clim.* **24**, 3484–3519 (2011).

Fan, J., Y. Wang, D. Rosenfeld, X. Liu: Review of Aerosol-Cloud Interactions: Mechanisms, Significance and Challenges: *J. Atmo. Sci.* 73(11), 4221-4252 (2016).

Gettelman, A. et al. High climate sensitivity in the Community Earth System Model Version 2 (CESM2), *Geophy. Res. Lett.*, **46**, 8329–8337 (2019).

Golaz, J.-C., Larson, V. E. & Cotton, W. R. A PDF-Based Model for Boundary Layer Clouds. Part II: Model Results. *J. Atmos. Sci.* **59**, 3552–3571 (2002).

Ghan, S. et al.: Challenges in constraining anthropogenic aerosol effects on cloud radiative forcing using present-day spatiotemporal variability. *Porc. Natl Acad. Sci.* USA. 113 (21): 5804-5811 (2016).

Hang, Y., L'Ecuyer, T. S., Henderson, D. S., Matus, A. V. & Wang, Z. Reassessing the effect of cloud type on earth's energy balance in the age of active spaceborne observations. Part II: Atmospheric heating. *J. Clim.* **32**, 6219–6236 (2019).

Hurrell, J. W. *et al.* The Community Earth System Model: A Framework for Collaborative Research. *Bull. Am. Meteorol. Soc.* **94**, 1339–1360 (2013).

IPCC. *Climate Change 2013: The Physical Science Basis. Contribution of Working Group I to the Fifth Assessment Report of the Intergovernmental Panel on Climate Change [Stocker, T.F., D. Qin, G.-K. Plattner, M. Tignor, S.K. Allen, J. Boschung, A. Nauels, Y. Xia,.* (Cambridge University Press, Cambridge, United Kingdom and New York, NY, USA, 2013). doi:10.1017/CBO9781107415324.

Jing, X. *et al.* A Multimodel Study on Warm Precipitation Biases in Global Models Compared to Satellite Observations. *J. Geophys. Res. Atmos.* **122**, 11,806-11,824 (2017).

Jing, X. & Suzuki, K. The Impact of Process-Based Warm Rain Constraints on the Aerosol Indirect Effect. *Geophys. Res. Lett.* **45**, 10,729-10,737 (2018).

Kay, J. E. *et al.* Scale-Aware and Definition-Aware Evaluation of Modeled Near-Surface Precipitation Frequency Using CloudSat Observations. *J. Geophys. Res.,* **123**, 4294–4309

(2018).
Kessler, E. On the Distribution and Continuity of Water Substance in Atmospheric Circulations. in *On the Distribution and Continuity of Water Substance in Atmospheric Circulations* 1–84 (American Meteorological Society, 1969). doi:10.1007/978-1-935704-36-2_1
Khairoutdinov, M. & Kogan, Y. A New Cloud Physics Parameterization in a Large-Eddy Simulation Model of Marine Stratocumulus. *Mon. Weather Rev.* **128**, 229–243 (2000).
Lau, K. M., & Wu H. T. Climatology and changes in tropical oceanic rainfall characteristics inferred from Tropical Rainffall Measuring Mission (TRMM) data (1998-2009). J. Geophys. Res. 116 D1711, doi:1029/2011D015827 (2011).
Lebsock, M., Morrison, H. & Gettelman, A. Microphysical implications of cloud-precipitation covariance derived from satellite remote sensing. *J. Geophys. Res.* **118**, 6521–6533 (2013).
L'Ecuyer, T. S., Hang, Y., Matus, A. V. & Wang, Z. Reassessing the effect of cloud type on earth's energy balance in the age of active spaceborne observations. Part I: Top of atmosphere and surface. *J. Clim.* **32**, 6197–6217 (2019).
Li, Z. et al. East Asian Study of Tropospheric Aerosols and Impact on Regional Cloud, Precipitation, and Climate (EAST-AIRCPC). *J. Geophys. Res.* **124***,* 2019JD030758 (2020).
Liu, Y., Daum, P. H., McGraw, R. L., Miller, M. A. & Niu, S. Theoretical expression for the autoconversion rate of the cloud droplet number concentration. *Geophys. Res. Lett.* **34**, (2007).
Liu, Y. & Daum, P. H. Parameterization of the Autoconversion Process.Part I: Analytical Formulation of the Kessler-Type Parameterizations. *J. Atmos. Sci.* **61**, 1539–1548 (2004).
Ma, X., Jia, H., Yu, F. & Quaas, J. Opposite Aerosol Index-Cloud Droplet Effective Radius Correlations Over Major Industrial Regions and Their Adjacent Oceans. *Geophys. Res. Lett.* **45**, 5771–5778 (2018).
Morrison, H. & Gettelman, A. A New Two-Moment Bulk Stratiform Cloud Microphysics Scheme in the Community Atmosphere Model, Version 3 (CAM3). Part I: Description and Numerical Tests. *J. Clim.* **21**, 3642–3659 (2008).
Minnis, P., et al. (2020). CERES MODIS cloud product retrievals for Edition 4 – Part I: Algorithm changes, *IEEE Trans. Geosci. Remote Sens.*, *58*, doi:10.1109/TGRS.2020.3008866.
Nakajima, T. Y. *et al.* Droplet Growth in Warm Water Clouds Observed by the A-Train. Part I: Sensitivity Analysis of the MODIS-Derived Cloud Droplet Sizes. *J. Atmos. Sci.* **67**, 1884–1896 (2010).
Penner, J.E., X. Dong**,** and Y. Chen: Observational evidence for a change in radiative forcing due to the indirect aerosol effect. *Nature*, ***427***, 231-234 (2004).
Rogers, R. R. R. & Yau, M. K. Short Course in Cloud Physics. 295 (1996).
Seinfeld, J.H. et al.: Improving our fundamental understanding of the role of aerosol−cloud interactions in the climate system. *Porc. Natl Acad. Sci.* USA. 113 (21): 5781-5790 (2016).
Stephens, G. L. *et al.* The albedo of earth. *Reviews of Geophysics* **53**, 141–163 (2015).
Stephens, G. L. Cloud Feedbacks in the Climate System: A Critical Review. *J. Clim.* **18**, 237–273 (2005).
Stephens, G. L. *et al.* Dreary state of precipitation in global models. *J. Geophys. Res.* **115,** (2010).
Schmidt, G. A. *et al.* Present-Day Atmospheric Simulations Using GISS ModelE: Comparison to In Situ, Satellite, and Reanalysis Data. *J. Clim.* **19**, 153–192 (2006).
Soden, B. J. & Vecchi, G. A. The vertical distribution of cloud feedback in coupled ocean-

atmosphere models. *Geophys. Res. Lett.* **38**, L12704 (2011).

Seinfeld, J.H. et al.: Improving our fundamental understanding of the role of aerosol−cloud interactions in the climate system. *Porc. Natl Acad. Sci.* USA. 113 (21): 5781-5790 (2016).

Suzuki, K., Stephens, G. L. & Lebsock, M. D. Aerosol effect on the warm rain formation process: Satellite observations and modeling. *J. Geophys. Res.* **118**, 170–184 (2013).

Suzuki, K. *et al.* Evaluation of the Warm Rain Formation Process in Global Models with Satellite Observations. *J. Atmos. Sci.* **72**, 3996–4014 (2015).

Suzuki, K., Nakajima, T., Nakajima, T. Y. & Stephens, G. L. Effect of the droplet activation process on microphysical properties of warm clouds. *Environ. Res. Lett.* **5**, 024012 (2010).

Takahashi, H., Lebsock, M., Suzuki, K., Stephens, G. & Wang, M. An investigation of microphysics and subgrid-scale variability in warm-rain clouds using the A-train observations and a multiscale modeling framework. *J. Geophys. Res.* **122**, 7493–7504 (2017).

Tripoli, G. J., Cotton, W. R., Tripoli, G. J. & Cotton, W. R. A Numerical Investigation of Several Factors Contributing to the Observed Variable Intensity of Deep Convection over South Florida. *J. Appl. Meteorol.* **19**, 1037–1063 (1980).

Wallace, J. M. & Hobbs, P. V. *Atmospheric Science: An Introductory Survey: Second Edition*. *Atmospheric Science: An Introductory Survey: Second Edition* (Elsevier Inc., 2006). doi:10.1016/C2009-0-00034-8

Wang, Y., Ma, P.-L., Jiang, J. H., Su, H. & Rasch, P. J. Toward reconciling the influence of atmospheric aerosols and greenhouse gases on light precipitation changes in Eastern China. *J. Geophys. Res. Atmos.* **121**, 5878–5887 (2016).

Wood, R. Drizzle in Stratiform Boundary Layer Clouds. Part I: Vertical and Horizontal Structure. *J. Atmos. Sci.* **62**, 3011–3033 (2005a).

Wood, R. Drizzle in Stratiform Boundary Layer Clouds. Part II: Microphysical Aspects. *J. Atmos. Sci.* **62**, 3034–3050 (2005b).

Wood, R. & Hartmann, D. L. Spatial variability of liquid water path in marine low cloud: The importance of mesoscale cellular convection. *J. Clim.* **19**, 1748–1764 (2006).

Wood, R., Kubar, T. L. & Hartmann, D. L. Understanding the Importance of Microphysics and Macrophysics for Warm Rain in Marine Low Clouds. Part II: Heuristic Models of Rain Formation. *J. Atmos. Sci.* **66**, 2973–2990 (2009).

Wood, R. Stratocumulus Clouds. *Mon. Weather Rev.* **140**, 2373–2423 (2012).

Wu, P., Dong, X. & Xi, B. Marine boundary layer drizzle properties and their impact on cloud property retrieval. *Atmos. Meas. Tech.* **8**, 3555–3562 (2015).

Wu, P. *et al.* Effects of environment forcing on marine boundary layer cloud-drizzle processes. *J. Geophys. Res.* **122**, 4463–4478 (2017).

Wu, P., Xi, B., Dong, X. & Zhang, Z. Evaluation of autoconversion and accretion enhancement factors in general circulation model warm-rain parameterizations using ground-based measurements over the Azores. *Atmos. Chem. Phys.* **18**, 17405–17420 (2018).

Wu, P., Dong, X., Xi, B., Tian, J. & Ward, D. M. Profiles of MBL Cloud and Drizzle Microphysical Properties Retrieved From Ground-Based Observations and Validated by Aircraft In Situ Measurements Over the Azores. *J. Geophys. Res.* **125**, (2020).

Xie, X., & Zhang, M. Scale-aware parameterization of liquid cloud inhomogeneity and its impact on simulated climate in CESM. *Journal of Geophysical Research: Atmospheres*, *120*(16), 8359–8371. https://doi.org/10.1002/2015JD023565 (2015).

Yamaguchi, T., Feingold, G. & Kazil, J. Stratocumulus to Cumulus Transition by Drizzle. *J. Adv. Model. Earth Syst.* **9**, 2333–2349 (2017).

Zhang, Z. *et al.* Subgrid variations of the cloud water and droplet number concentration over the tropical ocean: Satellite observations and implications for warm rain simulations in climate models. *Atmos. Chem. Phys.* **19**, 1077–1096 (2019).

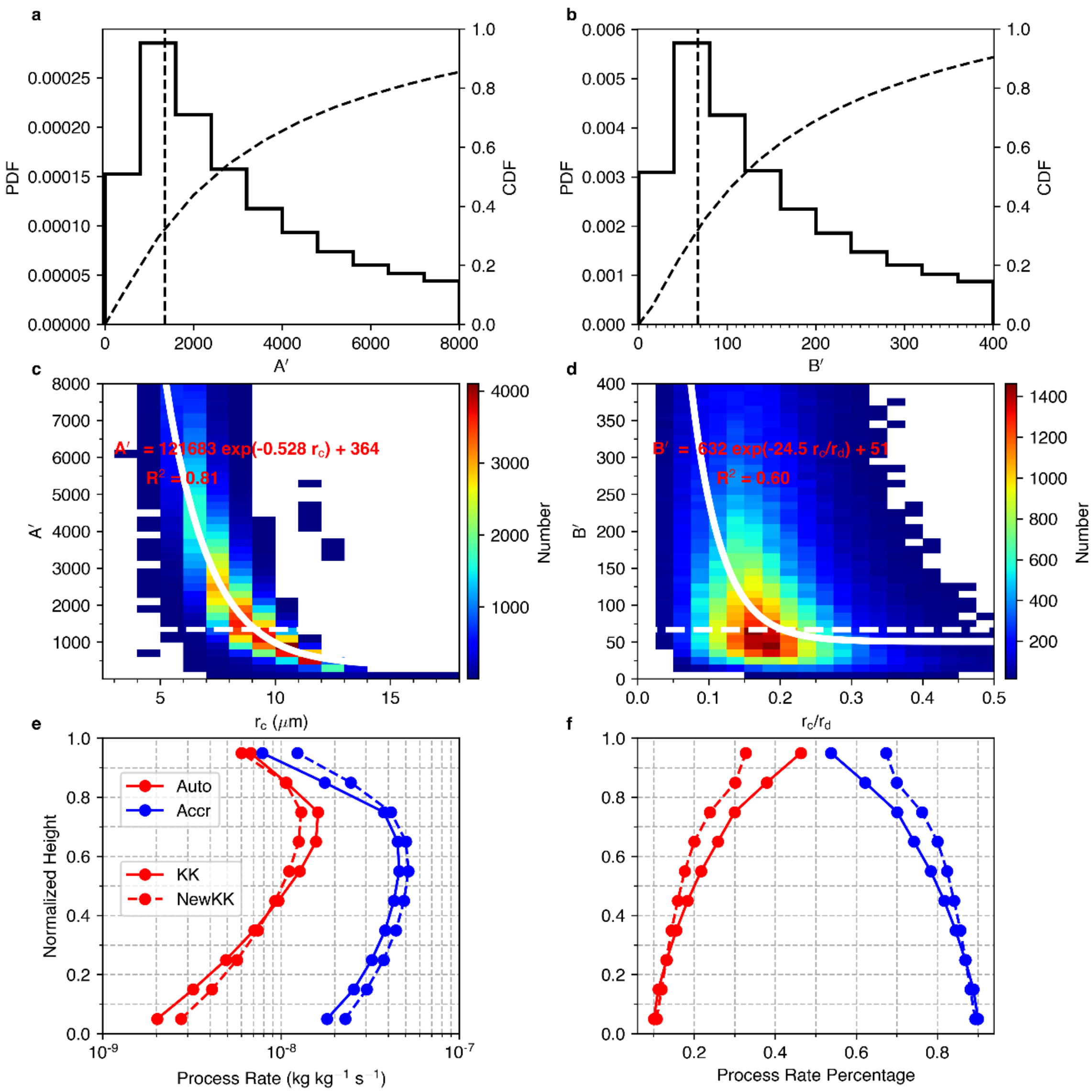

Fig. 1. (*a,b*) Probability density functions (PDFs, solid lines) and cumulative density functions (CDFs, dashed curves) of coefficients $A'(Z)$ and $B'(Z)$ calculated from ground-based retrievals. Vertical dashed lines mark the constants in the KK scheme. Joint histograms of (*c*) A'(Z) with r_c(Z) and (*d*) B'(Z) and the ratio of r_c(Z) to r_d(Z). White solid lines are the exponential fittings. White dashed lines mark the prescribed A and B in the KK scheme. (*e*) Normalized profiles of R_{auto} (red lines) and R_{accr} (blue lines) for all the drizzle cases during ACE-ENA (a total 9,213 1-min profiles) by cloud thickness ($z_i = \frac{z - z_b}{z_t - z_b}$, where subscripts b and t denote cloud base and top, respectively). The solid and dashed lines represent the profiles from KK and NKK schemes, respectively. (*f*) The percentages of total drizzle water production rate (R_{auto}+R_{accr}) contributed by R_{auto} and R_{accr}.

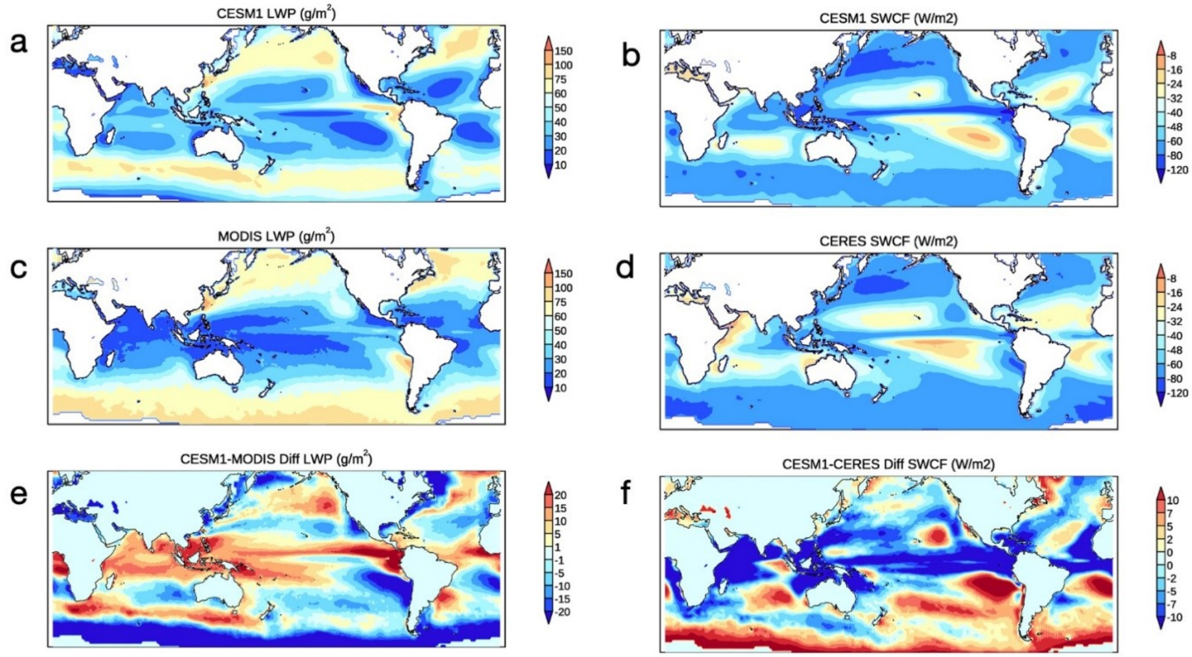

Fig. 2. Comparisons of cloud liquid water path (LWP, left column) and shortwave cloud forcing (SWCF, right column) between CESM1 present-day scenario simulations (a,b) and CERES-MODIS satellite cloud and radiation climatologies (c,d), as well as their differences (e,f). Model simulations consist of five ensemble members. Satellite data are averaged over 2001-2019 from both Terra and Aqua satellites.

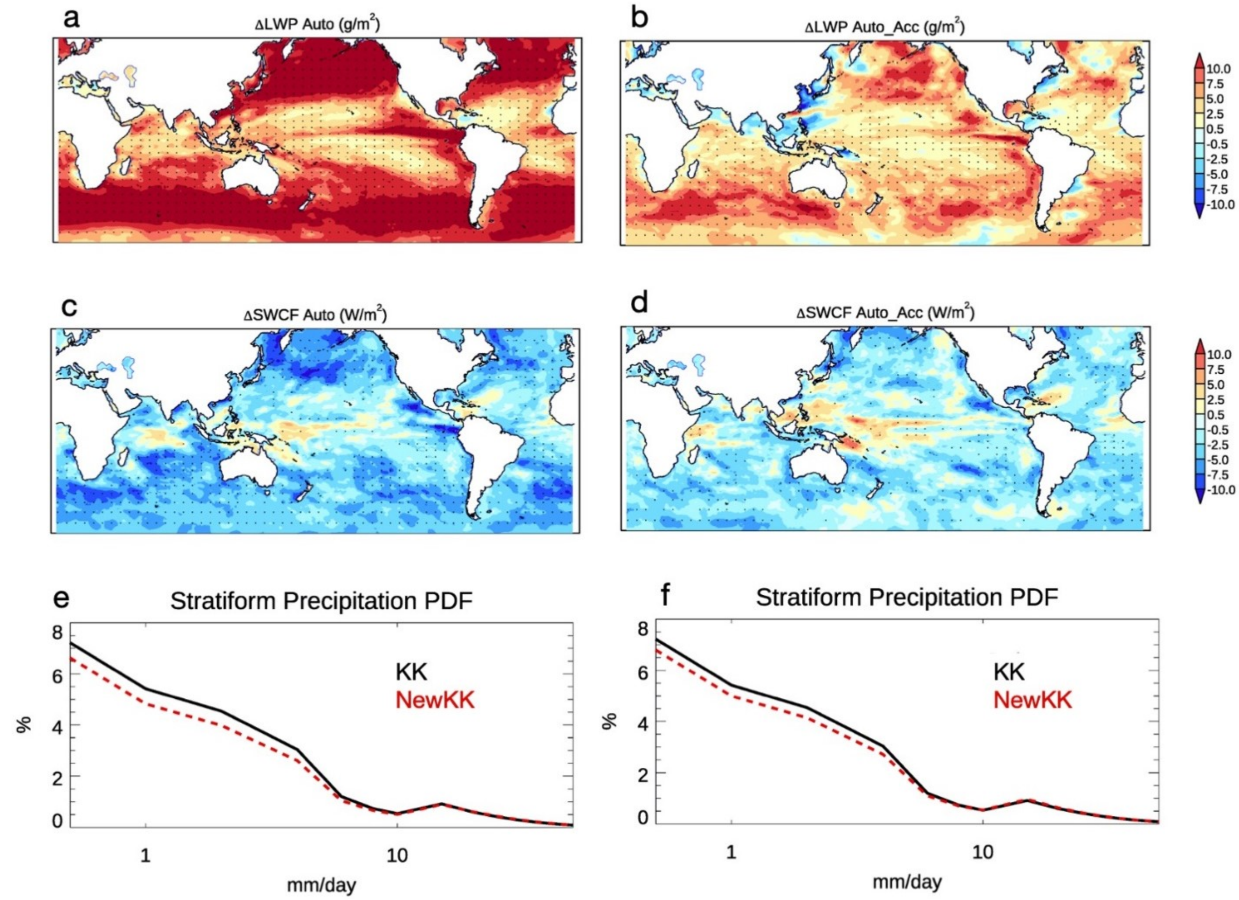

Fig. 3. Changes in LWP (a,b), SWCF (c,d), and Probability distribution functions (PDFs) of large-scale stratiform precipitation (e,f) in CESM simulations by different warm rain schemes (NKK – KK). Left column: autoconversion only. Right column: both autoconversion and accretion. The stippling indicates the statistically significant changes that are larger than the model internal variability (calculated as the standard deviation among the ensemble members). The precipitation PDF are averaged over 60ºS to 60ºN oceanic regions. The spreads of precipitation frequency in each bin are all less than 0.1% among different ensemble members, so they are too small to be shown in the panels e and f.